# Human Biodistribution and Radiation Dosimetry of $^{82}$Rb

Srinivasan Senthamizhchelvan, Paco E. Bravo, Caroline Esaias, Martin A. Lodge, Jennifer Merrill, Robert F. Hobbs, George Sgouros, and Frank M. Bengel

*Division of Nuclear Medicine, Russell H. Morgan Department of Radiology, Johns Hopkins University, Baltimore, Maryland*

Prior estimates of radiation-absorbed doses from $^{82}$Rb, a frequently used PET perfusion tracer, yielded discrepant results. We reevaluated $^{82}$Rb dosimetry using human in vivo biokinetic measurements. **Methods:** Ten healthy volunteers underwent dynamic PET/CT (6 contiguous table positions, each with separate $^{82}$Rb infusion). Source organ volumes of interest were delineated on the CT images and transferred to the PET images to obtain time-integrated activity coefficients. Radiation doses were estimated using OLINDA/EXM 1.0. **Results:** The highest mean absorbed organ doses ($\mu$Gy/MBq) were observed for the kidneys (5.81), heart wall (3.86), and lungs (2.96). Mean effective doses were 1.11 ± 0.22 and 1.26 ± 0.20 $\mu$Sv/MBq using the tissue-weighting factors of the International Commission on Radiological Protection (ICRP), publications 60 and 103, respectively. **Conclusion:** Our current $^{82}$Rb dosimetry suggests reasonably low radiation exposure. On the basis of this study, a clinical $^{82}$Rb injection of 2 × 1,480 MBq (80 mCi) would result in a mean effective dose of 3.7 mSv using the weighting factors of the ICRP 103—only slightly above the average annual natural background exposure in the United States (3.1 mSv).

**Key Words:** myocardium; imaging; $^{82}$Rb; positron emission tomography; dosimetry

**R**ecently, noninvasive imaging with radioisotopes and ionizing radiation has been increasingly scrutinized. As the number of noninvasive cardiovascular imaging procedures continues to increase, the concern over increased radiation exposure has also become an important issue (*1–3*). For $^{82}$Rb, the most frequently used clinical myocardial perfusion PET agent (*4–6*), discrepant absorbed dose estimates are given in the package insert (PI) of the CardioGen-82 generator (Bracco Diagnostics Inc.) (*7*) and a publication by the International Commission on Radiological Protection (ICRP) (*8*). Both reports have limitations. The PI lists relatively low absorbed dose estimates, which are based on data obtained for a limited number of source organs from 2 humans, by planar γ-camera (*9*), and from a rat biodistribution study (*10*). The significantly higher dose estimates in ICRP

53 (*8*) were not based on actual biokinetic measurements. In view of the short half-life of $^{82}$Rb (76.38 s), the ICRP 53 estimates were based on a model of relative blood flow to various tissues. ICRP 53 states that this may represent worst-case conditions for some organs because clearance or delayed uptake may yield lower cumulative activities (*8*).

The discrepancy between these $^{82}$Rb dose estimates remains unresolved, and uncertainty regarding actual dose from $^{82}$Rb imaging persists. Accordingly, we sought to provide definitive dose estimates, using multibed PET/CT of $^{82}$Rb in humans.

## MATERIALS AND METHODS

### Subjects

Ten healthy volunteers were included in the study (Table 1). Prescreening consisted of a detailed history, physical examination, and blood and urine samples. Subjects with evidence of clinical disease, history of organ-removal surgery (e.g., cholecystectomy, hysterectomy, splenectomy), or history of substance abuse were excluded. Individuals with a body mass index greater than 35 kg/m$^2$ and height greater than 1.80 m were also excluded because of practical issues with PET/CT. In female subjects, pregnancy was ruled out. The protocol was approved by the Johns Hopkins Institutional Review Board. All volunteers gave written informed consent.

### Study Design

Typically, radiotracer dosimetry involves serial longitudinal whole-body imaging after a single administration. Because of the short half-life of $^{82}$Rb, 6 tracer infusions (<740 MBq) were performed, each followed by dynamic PET at different body positions to cover all organs of interest.

### $^{82}$Sr/$^{82}$Rb Generator

A commercially available $^{82}$Sr/$^{82}$Rb generator, the CardioGen-82, was used. For quality control, the first eluted activity on each study day was discarded, and the calibration factor of the infusion system was adjusted. A preset $^{82}$Rb activity was eluted and measured in a dose calibrator (CRC15; Capintec, Inc.), at a time corresponding to 76 s from the end of infusion (EOI). Then, the ratio of measured activity in the dose calibrator, decay-corrected to EOI, and printed EOI activity of the generator were calculated. If the ratio was outside the 1.0 ± 0.05 limit, the procedure was repeated, and the calibration factor was adjusted until the ratio was within limits. The amount of strontium breakthrough at the end of elution was measured to ensure levels of $^{82}$Sr and $^{85}$Sr within recommended limits (<0.02 and <0.2 kBq/MBq of $^{82}$Rb, respectively) (*7*).

**TABLE 1.** Research Subject Characteristics

| Subject no. | Age (y) | Sex | Mass (kg) | Height (m) | Body mass index (kg/m$^2$) | Administered activity of $^{82}$Rb (MBq) per bed position (mean ± SD) |
|---|---|---|---|---|---|---|
| RB001 | 36 | F | 45 | 1.62 | 17.1 | 660 ± 3 |
| RB002 | 52 | M | 99 | 1.70 | 34.3 | 480 ± 2 |
| RB003 | 31 | M | 68 | 1.77 | 21.7 | 704 ± 3 |
| RB004 | 29 | M | 50 | 1.70 | 17.3 | 704 ± 3 |
| RB005 | 24 | F | 51 | 1.55 | 21.2 | 502 ± 3 |
| RB006 | 35 | M | 73 | 1.78 | 23.0 | 503 ± 3 |
| RB007 | 24 | M | 83 | 1.78 | 26.2 | 504 ± 3 |
| RB008 | 33 | F | 75 | 1.60 | 29.3 | 436 ± 2 |
| RB009 | 20 | F | 70 | 1.57 | 28.4 | 437 ± 2 |
| RB010 | 26 | F | 60 | 1.65 | 22.0 | 435 ± 2 |
| Mean ± SD | 31.0 ± 9.0 | | 67.4 ± 16.6 | 1.67 ± 0.1 | 24.1 ± 5.5 | 536 ± 100 |

## PET/CT

A Discovery Rx VCT scanner (GE Healthcare), equipped with high-performance lutetium-yttrium oxyorthosilicate PET crystals and a 64-slice CT component, was used. Subjects were positioned supine and imaged at rest. Six contiguous single-bed-position PET images were acquired in 2-dimensional mode, with 5 mm of overlap. For each position, helical transmission CT (120 kVp; 20–200 mA, automatically adjusted) was performed first. Then, PET was performed in list mode for 8 min, immediately after the start of intravenous infusion of 536 ± 100 MBq of $^{82}$Rb. List-mode data were resampled and iteratively reconstructed (ordered-subset expectation maximization; 21 subsets, 2 iterations) to attenuation-corrected dynamic sequences with 32 frames (20 × 6, 5 × 12, 4 × 30, and 3 × 60 s).

## Cross-Calibration of $^{82}$Rb Generator and PET/CT Scanner

A phantom study was performed to directly cross-calibrate the PET/CT scanner with the $^{82}$Rb generator infusion system. A water-filled cylindric phantom was connected to the $^{82}$Rb generator, and 1,480 MBq were infused. After mixing and positioning, 2-dimensional PET was started 76 s after EOI. Acquisition and reconstruction were done as described in the "PET/CT" section and repeated 3 times. The mean ratio of measured and actual activity concentration was 0.93 ± 0.01. A calibration factor of 0.93 was subsequently used in the absorbed dose calculations.

## Organ Contouring

MIMvista (version 4.2; MIMvista Corp.) was used to generate source organ contours on the CT images, with the aid of summed PET and fused PET/CT images (Figs. 1A and 1B). All organs expected for dose computation were delineated, except for muscle, thymus, and bone. Those were excluded either because they did not demonstrate uptake or because they could not be accurately delineated. For organs that extended beyond 1 bed position, separate contours were drawn at each position and summed afterward. Gastrointestinal organs were delineated into stomach contents, small intestine (SI) contents, upper large intestine (ULI) (ascending, transverse, descending colon) contents, and lower large intestine (LLI) (sigmoid, rectum) contents. Heart contents (blood pool in cavities) contour was obtained using the difference between contours drawn for the whole heart and those drawn for the heart wall (visualized ventricular myocardium) (Fig. 1C). Red bone marrow was delineated on the femoral head. Whenever a source organ could not be drawn completely, the average activity concentration was multiplied by a standard phantom–based organ volume-density product (11).

## Dosimetry

CT-derived organ contours were overlaid onto matching dynamic PET data to extract activity concentration. Organ volumes from CT were converted to mass using published density values (12,13). Organ content mass was obtained by multiplying volume by CT-measured density.

Decay corrections were reversed using decay factors from image headers. Activity concentration, normalized to administered activity, was plotted against time for each organ. The initial-tracer-uptake area under the curve was obtained by trapezoidal integration (14). Decay-phase area under the curve was obtained by exponential curve fit using SAAM-II (15). Time-integrated activity coefficients $\tilde{a}(r_S, \infty)$ were calculated pursuant to the MIRD Committee formalism (16):

$$\tilde{a}(r_S, \infty) = \int_0^\infty a(r_S, t)dt = \frac{1}{fA_0}\int_0^\infty A(r_S, t)dt, \qquad \text{Eq. 1}$$
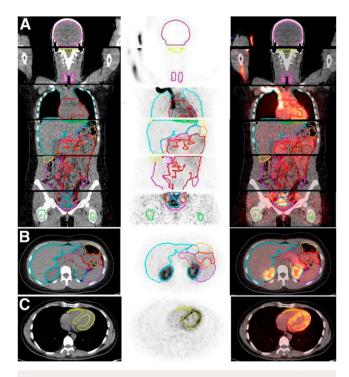
where $A_0$ is the administered activity (EOI activity from the generator), $f$ is the cross-calibration factor between the generator and scanner, $a(r_S, t)$ is the activity in the source organ $A(r_S, t)$ time ($t$) normalized to a unit administered activity ($A_0$).

Because no activity was excreted by the subjects during imaging, the time-integrated activity coefficient for the remainder of the body was calculated by subtracting the sum of the time-integrated activity coefficients of all source organs from the reciprocal of the $^{82}$Rb physical decay constant. If $A(r_S, t)$ is normalized to a unit administered activity ($A_0$) and denoted as $a(r_S, t)$, then the absorbed dose coefficient $d(r_T, \infty)$ in target organ ($r_T$) is given as:

$$d(r_T, \infty) = \sum_{r_S} \tilde{a}(r_S, \infty)S(r_T \leftarrow r_S), \qquad \text{Eq. 2}$$

where $S(r_T \leftarrow r_S)$ is the mean absorbed dose to target tissue ($r_T$) per unit administered activity. The OLINDA/EXM 1.0 dosimetry software was used to obtain absorbed dose estimates (17).

$^{82}$Rb activity observed in the gastrointestinal tract source regions (stomach, SI, ULI, and LLI) was due to blood flow to

**FIGURE 1.** Definition of organ contours on PET/CT images. (A) Coronal view of 6 bed positions stacked together (separated by transaxial lines), with color-coded organ contours on CT (left), PET (summed image of all dynamic frames, middle), and PET/CT fusion (right) images. (B) Transverse view of upper abdominal region with color-coded organ contours on CT, PET, and PET/CT fusion images. (C) Transverse view of heart region, with heart wall contours (yellow) shown on CT, PET (summed image of last 20 frames), and PET/CT fusion images.

these organ walls. OLINDA/EXM 1.0 calculates the gastrointestinal tract (stomach, SI, ULI, and LLI) wall doses by assuming that the activity is in the contents. Therefore, we corrected the OLINDA/EXM 1.0 dose estimates for gastrointestinal tract walls to reflect that the doses were from wall to wall and not from contents to wall. We assumed self-absorption of β-emissions originating in the gastrointestinal tract walls and added the dose contribution from all other source regions to this. The total β-emission energy per nuclear transformation ($\Delta = 2.26E-13$ Gy-kg/Bq-s) for $^{82}$Rb was used (18).

## RESULTS

### Biokinetics

The mean time–activity curves for source organs are shown in Figure 2. A brief delay of the initial appearance of activity is caused by the generator infusion time and time needed for the bolus to reach the respective organ. Lungs, as the first-pass organ, exhibited the highest transient activity concentration and peaked early. Activity concentration in heart content (blood pool) also peaked early, but the peak was lower than in the lungs, probably because of averaging of activity in all cavities and bolus dilution. Peak activity in the heart wall (myocardium) occurred 1 frame (6 s) after that in the lungs and heart content, but activity exceeded

lung and blood pool at later times because of myocardial retention. In the kidneys as the excreting organ, a broad peak of activity concentration was observed approximately 30 s after lung and heart activity had peaked. The liver as an alternative clearance pathway also showed a delayed peak, albeit at a lower overall level. Other organs showing significant $^{82}$Rb activity included the glandular organs (pancreas, thyroid, and adrenals) and the spleen, intestine, and stomach.

Source organ time-integrated activity coefficients are listed in Table 2. The organs with the highest mean time-integrated activity coefficient (in seconds) are the lungs, 10.8; kidneys, 7.0; liver, 6.2; and heart contents, 4.4. Breast contouring was not possible for subject RB001 because of implants. In the same subject, the ovaries and pancreas were not clearly visible on the CT image. For subject RB002, brain contouring was not possible because the brain was not sufficiently included in the 6 bed positions.

### Organ-Absorbed Doses

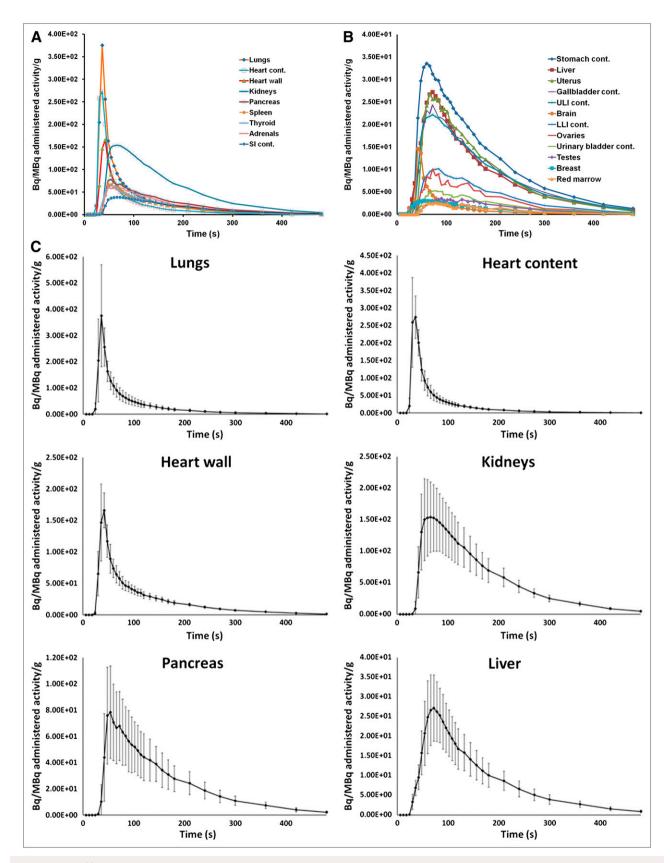Table 3 lists target organ–absorbed doses. The organs with the highest mean absorbed dose per unit administered activity (μGy/MBq) are the kidneys (5.81), heart wall (3.86), lungs (2.96), and pancreas (2.36). The absorbed dose to tissues listed in Table 3 that were not assigned a time-integrated activity coefficient reflects cross-fire photon contribution from organs that were assigned a time-integrated activity coefficient and contribution from activity assigned to the remainder of the body.

A comparison of mean organ-absorbed doses using the CardioGen-82 PI (7) and ICRP 53 (8) is shown in Table 4. Compared with ICRP 53, the CardioGen-82 PI showed significantly lower doses to most organs, except for the breast, heart wall, gonads, urinary bladder wall, and uterus. When compared with the CardioGen-82 PI, the ICRP 53 showed higher results for heart wall, lungs, and pancreas. The absorbed dose estimates for the kidneys as the critical organ in our analysis were 3- and 1.5-fold lower than the ICRP 53 and CardioGen-82 estimates, respectively.

### Effective Dose (ED)

The mean ED ± SD (1.11 ± 0.22 μSv/MBq) calculated by OLINDA/EXM 1.0 was based on ICRP 60 (19) tissue-weighting factors. ED was also calculated using the latest ICRP 103 tissue-weighting factors (20). Because ICRP 103 tissue-weighting factors are not yet implemented in OLINDA/EXM 1.0, we calculated ED directly using equivalent organ doses from the OLINDA/EXM 1.0 output. The sum of tissue-weighting factors for these target organs was 0.91 for men and 0.92 for women, instead of 1.0, because some organs contributing to ED are not listed in OLINDA/EXM 1.0. In obtaining ICRP 103–based ED, we accounted for these factors by scaling. An ED value of 1.26 ± 0.20 μSv/MBq was obtained.

The CardioGen-82 PI (7) does not list ED. If ED is calculated using organ doses listed in the PI and ICRP 60 (19) tissue-weighting factors are applied, the corresponding

**FIGURE 2.** [82]Rb organ time–activity curves plotted as activity concentration, normalized to administered activity for organs with high uptake (A) and organs with low uptake (B) (mean value of all subjects is shown at each time point) and selected source organs with high time-integrated activity coefficient (mean and SD are indicated at each time point) (C). cont. = contents.

**TABLE 2.** $^{82}$Rb Time-Integrated Activity Coefficient for Source Organs

| Source organ | Time-integrated activity coefficient (h) | | | | | | | | | | | | Coefficient of variation (%) |
| --- | --- | --- | --- | --- | --- | --- | --- | --- | --- | --- | --- | --- | --- |
| | RB001 | RB002 | RB003 | RB004 | RB005 | RB006 | RB007 | RB008 | RB009 | RB010 | Mean | SD | |
| Adrenals | 2.96E−05 | 4.10E−05 | 4.20E−05 | 4.34E−05 | 3.92E−05 | 1.48E−05 | 5.38E−05 | 3.74E−05 | 2.85E−05 | 4.73E−05 | 3.77E−05 | 1.10E−05 | 29 |
| Brain | 6.75E−05 | NA | 2.72E−04 | 2.54E−04 | 2.49E−04 | 1.17E−04 | 1.26E−04 | 2.31E−04 | 1.41E−04 | 1.68E−04 | 1.81E−04 | 7.30E−05 | 40 |
| Breasts | NA | NA | NA | NA | 3.98E−05 | NA | NA | 4.01E−05 | 7.18E−05 | 4.21E−05 | 4.84E−05 | 1.56E−05 | 32 |
| Gallbladder contents | 8.41E−05 | 1.68E−05 | 3.76E−05 | 5.37E−05 | 5.13E−05 | 2.15E−05 | 2.99E−05 | 7.95E−05 | 6.69E−05 | 1.09E−04 | 5.50E−05 | 2.99E−05 | 54 |
| LLI contents | 1.25E−04 | 2.58E−05 | 3.94E−05 | 7.41E−05 | 4.78E−05 | 1.30E−04 | 2.26E−05 | 5.17E−05 | 4.57E−05 | 6.90E−05 | 6.31E−05 | 3.75E−05 | 60 |
| SI contents | 1.26E−03 | 3.67E−04 | 4.24E−04 | 1.33E−03 | 8.06E−04 | 5.85E−04 | 4.49E−04 | 9.55E−04 | 5.03E−04 | 6.94E−04 | 7.38E−04 | 3.47E−04 | 47 |
| Stomach contents | 3.35E−04 | 4.15E−04 | 6.52E−04 | 1.65E−04 | 5.31E−04 | 1.22E−04 | 3.77E−04 | 2.90E−04 | 3.15E−04 | 3.96E−04 | 3.60E−04 | 1.57E−04 | 44 |
| ULI contents | 4.15E−04 | 1.13E−04 | 1.77E−04 | 3.43E−04 | 2.34E−04 | 1.76E−04 | 1.94E−04 | 2.21E−04 | 2.21E−04 | 2.65E−04 | 2.36E−04 | 8.75E−05 | 37 |
| Heart contents | 1.41E−03 | 1.11E−03 | 1.39E−03 | 1.39E−03 | 1.35E−03 | 9.93E−04 | 1.06E−03 | 1.13E−03 | 9.15E−04 | 1.41E−03 | 1.21E−03 | 1.92E−04 | 16 |
| Heart wall | 8.03E−04 | 6.82E−04 | 9.62E−04 | 9.96E−04 | 7.13E−04 | 8.27E−04 | 7.45E−04 | 7.72E−04 | 6.18E−04 | 8.24E−04 | 7.94E−04 | 1.17E−04 | 15 |
| Kidneys | 2.55E−03 | 1.31E−03 | 2.47E−03 | 2.12E−03 | 2.41E−03 | 9.19E−04 | 1.99E−03 | 1.76E−03 | 1.69E−03 | 2.24E−03 | 1.95E−03 | 5.31E−04 | 27 |
| Liver | 2.30E−03 | 1.43E−03 | 2.22E−03 | 2.31E−03 | 1.86E−03 | 9.57E−04 | 1.30E−03 | 1.58E−03 | 1.39E−03 | 1.84E−03 | 1.72E−03 | 4.65E−04 | 27 |
| Lungs | 3.20E−03 | 3.03E−03 | 2.78E−03 | 2.74E−03 | 3.12E−03 | 2.27E−03 | 2.84E−03 | 3.89E−03 | 2.86E−03 | 3.23E−03 | 3.00E−03 | 4.21E−04 | 14 |
| Ovaries | NA | NA | NA | NA | 2.13E−06 | NA | NA | 4.84E−06 | 2.61E−06 | 3.21E−06 | 3.20E−06 | 1.18E−06 | 37 |
| Pancreas | NA | 1.64E−04 | 1.77E−04 | 3.25E−04 | 3.63E−04 | 1.46E−04 | 2.88E−04 | 3.21E−04 | 2.29E−04 | 3.44E−04 | 2.62E−04 | 8.40E−05 | 32 |
| Red marrow | 3.27E−04 | 6.35E−05 | 1.12E−04 | 1.53E−04 | 5.20E−05 | 3.22E−05 | 7.04E−05 | 1.08E−04 | 1.14E−04 | 4.13E−05 | 1.07E−04 | 8.62E−05 | 80 |
| Spleen | 3.14E−04 | 2.97E−04 | 3.64E−04 | 6.18E−04 | 4.15E−04 | 1.54E−04 | 3.52E−04 | 3.49E−04 | 2.59E−04 | 3.73E−04 | 3.50E−04 | 1.19E−04 | 34 |
| Testes | NA | 8.24E−06 | 6.86E−06 | 6.26E−06 | NA | 2.98E−06 | 5.89E−06 | NA | NA | NA | 6.05E−06 | 1.93E−06 | 32 |
| Thyroid | 3.53E−05 | 2.37E−05 | 4.25E−05 | 7.03E−05 | 4.51E−05 | 3.41E−05 | 4.23E−05 | 6.25E−05 | 2.85E−05 | 3.19E−05 | 4.16E−05 | 1.47E−05 | 35 |
| Urinary bladder contents | 9.45E−05 | 2.86E−05 | 2.73E−05 | 4.97E−05 | 1.65E−05 | 2.77E−05 | 2.44E−05 | 5.73E−05 | 4.79E−05 | 2.39E−05 | 3.98E−05 | 2.34E−05 | 59 |
| Uterus | 1.78E−04 | NA | NA | NA | 3.93E−05 | NA | NA | 7.99E−05 | 5.44E−05 | 7.70E−05 | 8.57E−05 | 5.41E−05 | 63 |
| Remainder of body | 1.71E−02 | 2.15E−02 | 1.84E−02 | 1.76E−02 | 1.82E−02 | 2.31E−02 | 2.06E−02 | 1.86E−02 | 2.10E−02 | 1.84E−02 | 1.94E−02 | 1.97E−03 | 10 |

NA = not available.

**TABLE 3.** $^{82}$Rb Organ-Absorbed Dose per Unit Administered Activity

| Target organ | Absorbed dose (mGy/MBq) | | | | | | | | | | | | Coefficient of variation (%) |
|---|---|---|---|---|---|---|---|---|---|---|---|---|---|
| | RB001 | RB002 | RB003 | RB004 | RB005 | RB006 | RB007 | RB008 | RB009 | RB010 | Mean | SD | |
| Adrenals | 1.83E−03 | 2.07E−03 | 2.15E−03 | 2.22E−03 | 2.36E−03 | 8.35E−04 | 2.69E−03 | 2.24E−03 | 1.75E−03 | 2.79E−03 | 2.09E−03 | 5.50E−04 | 26 |
| Brain | 8.17E−05 | 3.00E−04 | 2.02E−04 | 1.89E−04 | 2.21E−04 | 1.05E−04 | 1.09E−04 | 2.08E−04 | 1.43E−04 | 1.59E−04 | 1.72E−04 | 6.57E−05 | 38 |
| Breasts | 3.53E−04 | NA | NA | NA | 1.83E−04 | NA | NA | 1.87E−04 | 2.52E−04 | 1.90E−04 | 2.33E−04 | 7.28E−05 | 31 |
| Gallbladder wall | 1.10E−03 | 4.99E−04 | 6.38E−04 | 7.51E−04 | 8.55E−04 | 5.40E−04 | 5.89E−04 | 1.06E−03 | 9.88E−04 | 1.30E−03 | 8.32E−04 | 2.72E−04 | 33 |
| LLI wall | 1.01E−03 | 4.60E−04 | 4.87E−04 | 6.59E−04 | 8.40E−04 | 9.95E−04 | 4.37E−04 | 6.54E−04 | 6.58E−04 | 7.33E−04 | 6.93E−04 | 2.06E−04 | 30 |
| SI | 2.13E−03 | 7.92E−04 | 8.32E−04 | 1.93E−03 | 1.23E−03 | 1.08E−03 | 8.89E−04 | 1.71E−03 | 9.88E−04 | 1.35E−03 | 1.29E−03 | 4.78E−04 | 37 |
| Stomach wall | 2.38E−03 | 2.52E−03 | 3.72E−03 | 1.20E−03 | 1.65E−03 | 1.01E−03 | 2.32E−03 | 2.14E−03 | 2.30E−03 | 2.75E−03 | 2.20E−03 | 7.81E−04 | 36 |
| ULI wall | 2.14E−03 | 7.74E−04 | 9.84E−04 | 1.62E−03 | 2.07E−03 | 1.04E−03 | 1.07E−03 | 1.34E−03 | 1.36E−03 | 1.51E−03 | 1.39E−03 | 4.56E−04 | 33 |
| Heart wall | 4.54E−03 | 3.05E−03 | 4.08E−03 | 4.17E−03 | 4.15E−03 | 3.32E−03 | 3.17E−03 | 4.13E−03 | 3.34E−03 | 4.62E−03 | 3.86E−03 | 5.81E−04 | 15 |
| Kidneys | 7.85E−03 | 3.76E−03 | 7.01E−03 | 6.05E−03 | 7.44E−03 | 2.66E−03 | 5.66E−03 | 5.46E−03 | 5.23E−03 | 6.93E−03 | 5.81E−03 | 1.64E−03 | 28 |
| Liver | 1.63E−03 | 7.79E−04 | 1.17E−03 | 1.21E−03 | 1.34E−03 | 5.47E−04 | 7.24E−04 | 1.16E−03 | 1.02E−03 | 1.33E−03 | 1.09E−03 | 3.28E−04 | 30 |
| Lungs | 3.45E−03 | 2.67E−03 | 2.46E−03 | 2.43E−03 | 3.36E−03 | 2.02E−03 | 2.50E−03 | 4.15E−03 | 3.08E−03 | 3.48E−03 | 2.96E−03 | 6.51E−04 | 22 |
| Muscle | 3.56E−04 | 3.29E−04 | 2.94E−04 | 2.85E−04 | 3.73E−04 | 3.48E−04 | 3.20E−04 | 3.79E−04 | 4.14E−04 | 3.75E−04 | 3.47E−04 | 4.05E−05 | 12 |
| Ovaries | 4.12E−04 | NA | NA | NA | 2.79E−04 | NA | NA | 4.71E−04 | 3.13E−04 | 3.54E−04 | 3.66E−04 | 7.69E−05 | 21 |
| Pancreas | 4.77E−04 | 1.57E−03 | 1.71E−03 | 2.97E−03 | 3.68E−03 | 1.39E−03 | 2.64E−03 | 3.26E−03 | 2.38E−03 | 3.50E−03 | 2.36E−03 | 1.05E−03 | 44 |
| Red marrow | 3.83E−04 | 2.89E−04 | 2.83E−04 | 2.92E−04 | 3.11E−04 | 2.91E−04 | 2.86E−04 | 3.30E−04 | 3.53E−04 | 3.08E−04 | 3.13E−04 | 3.32E−05 | 11 |
| Osteogenic cells | 5.81E−04 | 4.41E−04 | 4.00E−04 | 3.94E−04 | 5.32E−04 | 4.61E−04 | 4.28E−04 | 5.57E−04 | 6.15E−04 | 5.33E−04 | 4.94E−04 | 7.90E−05 | 16 |
| Skin | 3.10E−04 | 2.95E−04 | 2.59E−04 | 2.49E−04 | 3.28E−04 | 3.14E−04 | 2.86E−04 | 3.33E−04 | 3.70E−04 | 3.30E−04 | 3.07E−04 | 3.64E−05 | 12 |
| Spleen | 1.91E−03 | 1.48E−03 | 1.81E−03 | 2.96E−03 | 2.48E−03 | 8.15E−04 | 1.74E−03 | 2.10E−03 | 1.60E−03 | 2.24E−03 | 1.91E−03 | 5.86E−04 | 31 |
| Testes | NA | 2.29E−04 | 1.94E−04 | 1.81E−04 | NA | 1.29E−04 | 1.81E−04 | NA | NA | NA | 1.83E−04 | 3.59E−05 | 20 |
| Thymus | 4.11E−04 | 3.75E−04 | 3.46E−04 | 3.34E−04 | 4.26E−04 | 3.91E−04 | 3.63E−04 | 4.35E−04 | 4.60E−04 | 4.34E−04 | 3.98E−04 | 4.22E−05 | 11 |
| Thyroid | 1.67E−03 | 9.65E−04 | 1.66E−03 | 2.69E−03 | 2.12E−03 | 1.36E−03 | 1.66E−03 | 2.90E−03 | 1.37E−03 | 1.52E−03 | 1.79E−03 | 6.07E−04 | 34 |
| Urinary bladder wall | 5.92E−04 | 3.84E−04 | 3.40E−04 | 3.80E−04 | 3.81E−04 | 4.09E−04 | 3.66E−04 | 5.04E−04 | 5.15E−04 | 4.06E−04 | 4.28E−04 | 8.11E−05 | 19 |
| Uterus | 1.94E−03 | NA | NA | NA | 5.18E−04 | NA | NA | 9.36E−04 | 6.72E−04 | 9.00E−04 | 9.93E−04 | 5.56E−04 | 56 |
| Total body | 5.31E−04 | 4.21E−04 | 4.18E−04 | 4.19E−04 | 5.33E−04 | 4.22E−04 | 4.21E−04 | 5.36E−04 | 5.38E−04 | 5.33E−04 | 4.77E−04 | 6.01E−05 | 13 |
| Effective dose* (mSv/MBq) | 1.50E−03 | 1.11E−03 | 1.34E−03 | 1.13E−03 | 1.34E−03 | 8.52E−04 | 1.14E−03 | 1.48E−03 | 1.25E−03 | 1.45E−03 | 1.26E−03 | 2.04E−04 | 16 |

*Effective dose was calculated using ICRP 103 tissue-weighting factors.
NA = not applicable.

**TABLE 4.** Comparison of Mean Organ-Absorbed Doses with CardioGen-82 PI and ICRP 53

| Target organ | Absorbed dose (cGy) per 2,220 MBq of administered activity | | |
| --- | --- | --- | --- |
| | Current study | CardioGen-82 PI | ICRP 53 |
| Adrenals | 4.65E−01 | 2.20E−01 | 4.44E+00 |
| Brain | 3.81E−02 | NA | NA |
| Breasts | 5.17E−02 | NA | 4.22E−02 |
| Gallbladder wall | 1.85E−01 | NA | NA |
| LLI wall | 1.54E−01 | 1.90E−01 | 8.66E−01 |
| SI | 2.87E−01 | 3.20E−01 | 8.66E−01 |
| Stomach wall | 4.88E−01 | 1.90E−01 | 8.44E−01 |
| ULI wall | 3.09E−01 | 1.90E−01 | 8.66E−01 |
| Heart wall | 8.56E−01 | 4.20E−01 | 7.33E−01 |
| Kidneys | 1.29E+00 | 1.92E+00 | 4.00E+00 |
| Liver | 2.42E−01 | 1.90E−01 | 2.15E−01 |
| Lungs | 6.57E−01 | 3.80E−01 | 5.33E−01 |
| Muscle | 7.71E−02 | NA | NA |
| Ovaries | 8.12E−02 | 8.40E−02 | 5.33E−02 |
| Pancreas | 5.23E−01 | 1.40E−01 | 9.99E−01 |
| Red marrow | 6.94E−02 | 8.40E−02 | 2.20E−01 |
| Osteogenic cells | 1.10E−01 | NA | 1.49E−01 |
| Skin | 6.82E−02 | NA | NA |
| Spleen | 4.25E−01 | NA | 1.11E+00 |
| Testes | 4.06E−02 | 6.6E−02 | 2.89E−02 |
| Thymus | 8.82E−02 | NA | NA |
| Thyroid | 3.98E−01 | NA | 8.44E+00 |
| Urinary bladder wall | 9.49E−02 | NA | 3.77E−02 |
| Uterus | 2.20E−01 | NA | 4.66E−02 |
| Total body | 1.06E−01 | 9.60E−02 | NA |

NA = not available.

ED is 2.4 mSv for 2,960 MBq (80 mCi) (2). Our current ED estimate based on ICRP 60 is 38% higher than that from the PI. ICRP 53 lists only ED equivalent. In an addendum to ICRP 53 (21), the ED is calculated using ICRP 60 tissue-weighting factors. Our current ED, based on ICRP 60, is 33% of that given in the addendum to ICRP 53 (21).

## DISCUSSION

It is likely that the clinical application of $^{82}$Rb and PET for myocardial perfusion imaging will continue to grow. The results of our study resolve a discrepancy in radiation exposure resulting from 2 prior dose estimates, with inherent limitations. Using a multibed, multiinjection PET/CT protocol, we measured human in vivo biodistribution of $^{82}$Rb in all relevant source organs. The resulting absorbed dose and ED estimates obtained were generally lower than ICRP 53 values and generally higher than values reported in the CardioGen-82 PI.

Differences with ICRP can be explained by its conservative model, which, instead of using biokinetic measurements, used relative organ blood flow to define uptake and physical decay to define washout. The highest organ-absorbed dose in our study was to the kidneys; however, the dose was still 3-fold lower than in ICRP 53. Our in vivo biokinetics show that peak activity in the kidneys does not occur until approximately 45 s after infusion. This delay provides a partial explanation for the large difference between the current absorbed dose estimate and that in ICRP 53. The most significant difference between ICRP 53 and the current study is for thyroid and adrenals, which were 21- and 10-fold lower for our study than for ICRP 53. Heart wall and lung absorbed dose estimates were slightly higher.

Differences with the CardioGen-82 PI may be explained by the fact that most of the organ-absorbed doses are calculated from biokinetics measured using a γ-camera (9). Inaccuracy in quantifying activity in the lungs using a γ-camera and the unavoidably crude separation of heart chamber from wall activity may explain the nearly 2-fold lower organ dose estimates. Additionally, the dose estimate for testes was based on 1 subject. However, the ovary dose estimate was extrapolated from male-to-female comparisons, and dose estimates for some organs were not obtained. Absorbed dose estimates for the brain and gallbladder wall are included in the present study; these have not been previously reported. Absorbed dose estimates for gastrointestinal tract walls in our study were obtained by assuming total self-absorption of β-emissions—an overly conservative assumption because $^{82}$Rb has highly energetic β-(positron) emissions, and not all energy emitted is completely absorbed inside the thin gastrointestinal tract walls.

Other published reports to date providing $^{82}$Rb dosimetry have used the data of Ryan et al. (9) and the ICRP data as sources for dosimetry calculations or compilations (2,3,22). In addition to these 2 primary data sources, Kearfott (10) used rat biodistribution data to provide $^{82}$Rb dosimetry. On the basis of our present study, a standard clinical $^{82}$Rb injection of 2 × 1,480 = 2,960 MBq (2 × 40 = 80 mCi) would result in a mean ED of 3.7 mSv using the newly published ICRP 103 tissue-weighting factors. This ED is only slightly above the 3.1-mSv average annual natural background exposure in the United States (23). The additional dose from a transmission measurement for attenuation correction would need to be added (∼0.3 mSv for the cardiac region in our protocol) to obtain total ED from a clinical PET/CT procedure.

An in-depth comparison with other cardiac imaging procedures is beyond the scope of this study. EDs for cardiac perfusion imaging agents have recently been summarized elsewhere in the literature (2) for clinically administered activities. Our current dosimetry places $^{82}$Rb in the same low range as alternative PET perfusion tracers. It also provides further evidence that PET is at the lower end of ED among cardiac imaging procedures that involve ionizing radiation.

## CONCLUSION

This study provides dose estimates for $^{82}$Rb based on quantitative whole-body biokinetics in humans. Results

suggest a reasonably low radiation exposure. The data obtained from this study provide a scientific basis for the ongoing discussion of radiation exposure from cardiac imaging procedures.

## REFERENCES

1. Thompson RC, Cullom SJ. Issues regarding radiation dosage of cardiac nuclear and radiography procedures. *J Nucl Cardiol.* 2006;13:19–23.
2. Einstein AJ, Moser KW, Thompson RC, Cerqueira MD, Henzlova MJ. Radiation dose to patients from cardiac diagnostic imaging. *Circulation.* 2007;116:1290–1305.
3. Stabin MG. Radiopharmaceuticals for nuclear cardiology: radiation dosimetry, uncertainties, and risk. *J Nucl Med.* 2008;49:1555–1563.
4. Di Carli MF, Hachamovitch R. New technology for noninvasive evaluation of coronary artery disease. *Circulation.* 2007;115:1464–1480.
5. Bengel FM, Higuchi T, Javadi MS, Lautamaki R. Cardiac positron emission tomography. *J Am Coll Cardiol.* 2009;54:1–15.
6. Heller GV, Calnon D, Dorbala S. Recent advances in cardiac PET and PET/CT myocardial perfusion imaging. *J Nucl Cardiol.* 2009;16:962–969.
7. CardioGen-82 [package insert]. Princeton, NJ: Bracco Diagnostics Inc.; 2000.
8. International Commission on Radiological Protection (ICRP). *Radiation Dose to Patients from Radiopharmaceuticals.* ICRP publication 53. New York, NY: Pergamon Press; 1988.
9. Ryan J, Harper P, Stark V, Peterson E, Lathrop K. Radiation absorbed dose estimate for Rb-82 using in vivo measurements in man [abstract]. *J Nucl Med.* 1984;25:94P.
10. Kearfott KJ. Radiation absorbed dose estimates for positron emission tomography (PET): K-38, Rb-81, Rb-82, and Cs-130. *J Nucl Med.* 1982;23:1128–1132.
11. Cristy M, Eckerman K. *Specific Absorbed Fractions of Energy at Various Ages from Internal Photons Sources.* Oak Ridge, TN: Oak Ridge National Laboratory; 1987:V1–V7. ORNL/TM-8381.
12. International Commission on Radiation Units and Measurements (ICRU). *Tissue Substitutes in Radiation Dosimetry and Measurement.* Report no. 44. Bethesda, MD: ICRU; 1989.
13. International Commission on Radiological Protection (ICRP). *Basic Anatomical and Physiological Data for Use in Radiological Protection: Reference Values.* ICRP publication 89. Oxford, U.K.: Pergamon Press; 2002.
14. William HP, Saul AT, William TV, Brian PF. *Numerical Recipes in C: The Art of Scientific Computing.* 2nd ed. Cambridge University Press; 1992.
15. Barrett PH, Bell BM, Cobelli C, et al. SAAM II: simulation, analysis, and modeling software for tracer and pharmacokinetic studies. *Metabolism.* 1998;47:484–492.
16. Bolch WE, Eckerman KF, Sgouros G, Thomas SR. MIRD pamphlet no. 21: a generalized schema for radiopharmaceutical dosimetry-standardization of nomenclature. *J Nucl Med.* 2009;50:477–484.
17. Stabin MG, Sparks RB, Crowe E. OLINDA/EXM: the second-generation personal computer software for internal dose assessment in nuclear medicine. *J Nucl Med.* 2005;46:1023–1027.
18. Eckerman KF, Enzo A. *MIRD: Radionuclide Data and Decay Schemes.* 2nd ed. Reston, VA: The Society of Nuclear Medicine; 2008.
19. International Commission on Radiological Protection (ICRP). *1990 Recommendations of the International Commission on Radiological Protection.* ICRP publication 60. New York, NY: Pergamon Press; 1991.
20. International Commission on Radiological Protection (ICRP). *2007 Recommendations of the International Commission on Radiological Protection.* ICRP publication 103. Burlington, MA: Elsevier; 2008.
21. International Commission on Radiological Protection (ICRP). *Radiation Dose to Patients from Radiopharmaceuticals.* ICRP publication 80, addendum 2 to ICRP Publication 53. Oxford, U.K.: Pergamon Press; 1999.
22. Leggett RW, Williams LR. A proposed blood circulation model for reference man. *Health Phys.* 1995;69:187–201.
23. National Council on Radiation Protection and Measurements (NCRP). *Ionizing Radiation Exposure of the Population of the United States.* Report no. 160. Bethesda, MD: NCRP; 2009.